Electronic structure and thermoelectric properties of skutterudite compounds

2004 J. Phys.: Condens. Matter 16 979

(http://iopscience.iop.org/0953-8984/16/6/025)

INSTITUTE OF PHYSICS PUBLISHING JOURNAL OF PHYSICS: CONDENSED MATTER

J. Phys.: Condens. Matter **16** (2004) 979–987 PII: S0953-8984(04)65431-2

Electronic structure and thermoelectric properties of skutterudite compounds

E Z Kurmaev[1], A Moewes[2], I R Shein[3], L D Finkelstein[1], A L Ivanovskii[3] and H Anno[4]

[1] Institute of Metal Physics, Russian Academy of Sciences—Ural Division, 620219 Yekaterinburg GSP-170, Russia
[2] Department of Physics and Engineering Physics, University of Saskatchewan, 116 Science Place, Saskatoon, Saskatchewan S7N 5E2, Canada
[3] Institute of Solid State Chemistry, Russian Academy of Sciences—Ural Division, 620219 Yekaterinburg GSP-145, Russia
[4] Tokyo University of Science, Yamaguchi, 1-1-1 Daigaku-dori, Onoda 756-0884, Japan

Received 1 July 2003
Published 30 January 2004
Online at stacks.iop.org/JPhysCM/16/979 (DOI: 10.1088/0953-8984/16/6/025)

Abstract

We present soft x-ray fluorescence measurements of skutterudite compounds ($CoAs_3$ and $CoSb_3$). Our results are compared with x-ray photoelectron spectra (XPS) and band structure calculations. The occupancy of d states is found to increase in transition metal antimonides with respect to that of pure metals. The experimental spectra are interpreted in terms of our LDA band structure calculations and we find that electron correlation does not have to be taken into account. The intensity ratio of the Co L_2 to L_3 emission lines is found to be 0.20 and 0.15 for $CoAs_3$ and $CoSb_3$, respectively, which we attribute to the decrease in Coster–Kronig processes in $CoAs_3$ compared to $CoSb_3$ with its smaller carrier density. The calculated values of the thermoelectric figures of merit show that $CoSb_3$ is the most promising thermoelectric material, which is in accordance with experimental measurements of the electrical conductivity and Seebeck coefficient.

Developing a cooling technology that avoids the use of greenhouse gases reducing ozone and toxic or otherwise hazardous materials is of obvious interest. More environmentally friendly techniques make use of thermoelectric [1] or magnetic [2] refrigeration. Conventional thermoelectric refrigerators with bismuth telluride alloys suffer from low efficiencies compared to common compressor-based refrigerators. Thermoelectric refrigerators are currently put to use where reliability is more important than economical aspects, for example for cooling for computer processing units or infrared detectors. Developing more efficient thermoelectric materials is of extreme interest. In order to be used in more efficient thermoelectric systems, a material should offer high electrical conductivity σ, low thermal conductivity κ and a high

Table 1. Calculated and experimental values of band gaps for $CoSb_3$ and $CoAs_3$.

Sample	Band gap (calc.) (eV)	Band gap (exper.) (eV)
$CoSb_3$	0.05 [6]	0.03 [10]
	0.22 [7]	0.05 [11]
	0.07 [12]	
	0.140 (present)	0 (present)
$CoAs_3$	0 [6]	0.25 [13]
	0.072 (present)	
$RhSb_3$	0 (present)	

Seebeck coefficient S. Skutterudites of MA_3 type (with M being Co, Rh, Ir and A standing for P, As, Sb) satisfy these requirements and therefore are considered promising candidate advanced thermoelectric materials [3]. It is widely expected that the thermoelectric properties of binary skutterudites can be manipulated and hence optimized by alloying or by inserting heavy neutral atoms that fill the large voids that exist in skutterudite crystal structures. In order to accomplish this most efficiently, it is essential to understand the electronic structure of binary skutterudites in detail.

Among skutterudites compounds, $CoSb_3$ has been of special interest because of the relatively high thermoelectric figure of merit ($Z = \sigma S^2/\kappa$) favouring its use for thermoelectric applications at high temperatures [3, 4]. A first electronic bonding model attempting to explain qualitatively semiconducting and diamagnetic properties of these compounds was suggested in [5]. Singh and Pickett [6] reported self-consistent band structure calculations for $CoAs_3$, $CoSb_3$ and $IrSb_3$ using the linearized augmented-plane-wave (LAPW) method. According to these calculations, linear band dispersion near the Fermi level causes the unusual transport properties of skutterudites. Other calculations [7] suggest a band structure of $CoSb_3$ that is typical of a narrow gap semiconductor. It is supposed that the effective mass of charge carriers in the $CoSb_3$ conduction band as deduced from band structure calculations [7] is ten times smaller than that estimated from transport experiments [8]. The calculated band gap values differ strongly from experimental values as shown in table 1. This is due to the well-known underestimation of the band gap in the local density approximation (LDA). Some characteristics of skutterudites are not well described by the conventional band approach. Electron correlations might have to be taken into account. In order to conclude from electronic structure calculations as to the thermoelectric properties of skutterudites the calculations ought to be compared with experimental valence band spectra. In the present paper we report the first x-ray fluorescence measurements on $CoAs_3$ and $CoSb_3$. X-ray emission and photoelectron [9] valence spectra of $CoAs_3$, $CoSb_3$ and $RhSb_3$ are compared with band structure calculations.

The x-ray fluorescent measurements were performed on Beamline 8.0.1 at the Advanced Light Source (ALS) at Lawrence Berkeley National Laboratory employing the soft x-ray fluorescence end-station [14]. The emitted radiation is dispersed using a Rowland circle type spectrometer with spherical gratings and analysed by a photon-counting area sensitive multichannel plate. Co $L_{2,3}$ ($3d4s \rightarrow 2p$ transition) and Rh $M_{4,5}$ ($5p \rightarrow 3d$ transition) x-ray fluorescent emission spectra were measured using two different diffraction gratings ($R = 10$ m and $N = 1500$ and 600 lines mm^{-1}, respectively).

We have used a scalar relativistic self-consistent full-potential LMTO method within the local density approximation (LDA) [15, 16] for our band structure calculations of $CoAs_3$, $CoSb_3$ and $RhSb_3$. The tetrahedron method was applied to calculate the density of states (DOS) and the dispersion curves $E(\mathbf{k})$ used 550 irreducible $\mathbf{k}$-points.

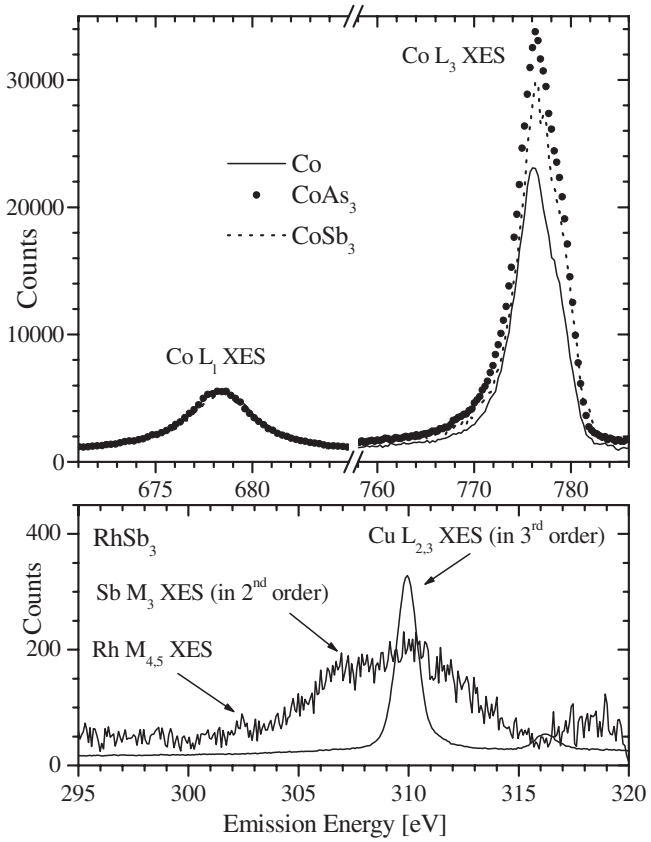

Figure 1. Co L_1 and L_3 XES of Co, $CoAs_3$ and $CoSb_3$ (top) and Rh $M_{4,5}$ XES of $RhSb_3$ (bottom).

Table 2. The orbital occupancy of cobalt atoms in Co, $CoAs_3$ and $CoSb_3$.

	4s	4p	3d
Co	0.3461	0.3320	6.9861
$CoAs_3$	0.3530	0.4608	7.2166
$CoSb_3$	0.3739	0.4558	7.3600

Figure 1 shows Co L_3 soft x-ray emission spectra (XES) of Co, $CoAs_3$ and $CoSb_3$ (upper panel). Co L_3 (VB $3d4s \rightarrow 2p_{3/2}$ transition) valence band spectra are normalized to the intensity of the Co L_1 ($3s \rightarrow 2p_{3/2}$ transition), which does not participate in the chemical bonding. The comparison reveals that the integral Co L_3 intensity is higher for antimonides than for pure metal. We attribute this to the higher Co 3d occupancy for compounds compared to that for metal. This argument is supported by the calculated Co 3d orbital occupancy as tabulated in table 2 for pure metal, $CoAs_3$ and $CoSb_3$.

We tried to detect the Rh $M_{4,5}$ ($5p \rightarrow 3d$ transition) XES for $RhSb_3$ but failed (see figure 1, upper panel) because of the extremely low intensity associated with this line and its overlap with Sb M_3 transitions ($4s \rightarrow 3p$).

At non-resonant excitation (when the excitation energy is far above threshold), the L_2 and L_3 spectra corresponding to the transitions $3d4s \rightarrow 2p_{1/2}$ and $3d4s \rightarrow 2p_{3/2}$ are excited

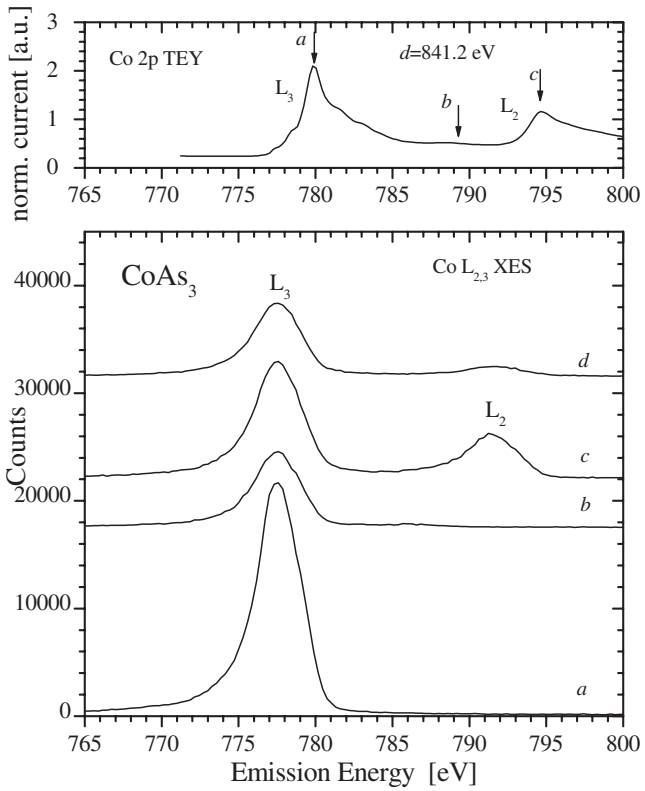

Figure 2. The excitation energy dependence of Co $L_{2,3}$ XES of $CoAs_3$.

simultaneously. In order to exclude this effect in our further considerations, we have measured the excitation energy dependence of Co $L_{2,3}$ emission of $CoAs_3$ and $CoSb_3$ with incoming photons between 778.5 and 841 eV. In figures 2 and 3, the corresponding excitation energies for the emission spectra (bottom graph) are labelled using arrows in the Co 2p x-ray absorption spectra (top graph). The absorption spectra were measured in the total electron yield (TEY) mode. When selectively excited at L_3 threshold, the Co L_3 XES (curve *a*) does not overlap with Co L_2 XES and thus gives an undistorted distribution of the occupied Co 3d density of states (DOS).

Figure 4 compares the ratio of intensities for Co L_2 to L_3 lines, $I(L_2)/I(L_3)$, for resonant excitation and in the non-resonant regime. The ratio $I(L_2)/I(L_3)$ deviates from the value of 0.5, which is expected from the occupancies for $j = 3/2$ and $1/2$. In both cases the ratio is higher for $CoAs_3$ than for $CoSb_3$. It is supposed that in 3d metals and alloys the ratio $I(L_2)/I(L_3)$ is smaller than 0.5 due to competing $L_2L_3M_{4,5}$ Coster–Kronig (CK) processes [17] and due to higher self-absorption of L_2 radiation (compared to L_3 radiation). The intensity ratio $I(L_2)/I(L_3)$ is generally higher for 3d oxides than for 3d metals because of the presence of additional CK mechanisms in metals involving many-electron processes in the valence band such as plasma vibrations and creation of multiple electron–hole pairs [18]. Following these arguments, we conclude that the $I(L_2)/I(L_3)$ ratio is higher in $CoAs_3$ because the Coster–Kronig process is suppressed due to its carrier density being lower than in $CoSb_3$ (see table 3).

The comparison of x-ray photoelectron spectra of the valence band (XPS VB) and x-ray emission spectra of $CoAs_3$, $CoSb_3$ and $RhSb_3$ are shown in figure 5. In order to convert the

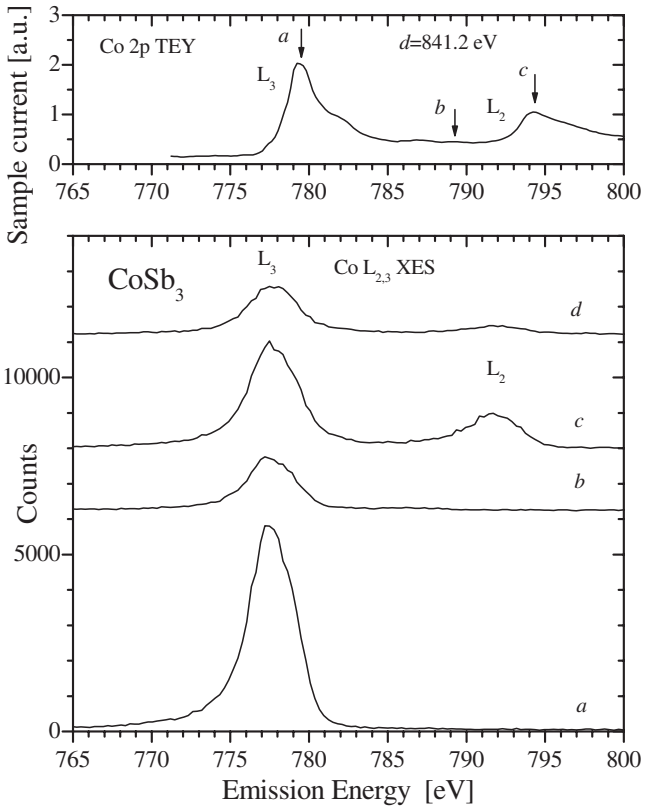

Figure 3. The excitation energy dependence of Co $L_{2,3}$ XES of $CoSb_3$.

Table 3. The calculated values of the Seebeck coefficient and Z factor.

Compound	S (exper.) (at ∼320 K) (μV K^{-1})	S (theor.) (0 K) (μV K^{-1})	σ (exper.) (at ∼290 K) (S cm^{-1})	σS^2 (μV)^2 (cm^{-1} K^{-2})
$CoAs_3$	166	134.7	427	7.9×10^6
$CoSb_3$	142	139.7	796	16×10^6
$RhSb_3$	80	111.7	2992	38×10^6

Co L_3 and Rh M_5 XES to the binding energy scale, we have subtracted the emission energy from the XPS binding energies of Co $2p_{3/2}$ and Rh $3d_{5/2}$ (see [5]). The top of the valence band of $CoAs_3$ and $CoSb_3$ has predominantly Co 3d character. The Sb 5p and As 4p states reside at lower binding energies and the atomic-like Sb 5s and As 4s states are situated further below.

The calculated band structures of $CoAs_3$, $CoSb_3$ and $RhSb_3$ are displayed in figures 6–8, respectively. The lower set of bands from −13 to −8 eV for $CoSb_3$ and $RhSb_3$ and from −15.2 to −10 eV for $CoAs_3$ originate from Sb 5s and As 4s states, respectively. Hybridized transition metal d and nonmetallic p states contribute to the region from −6 eV up to the Fermi level. We note that the density of states distribution in the vicinity of the Fermi level is different for $CoAs_3$, $CoSb_3$ and $RhSb_3$. In both Co-containing compounds, Co 3d states dominate near the top of the valence band, whereas in $RhSb_3$, the Rh 4d states reside at

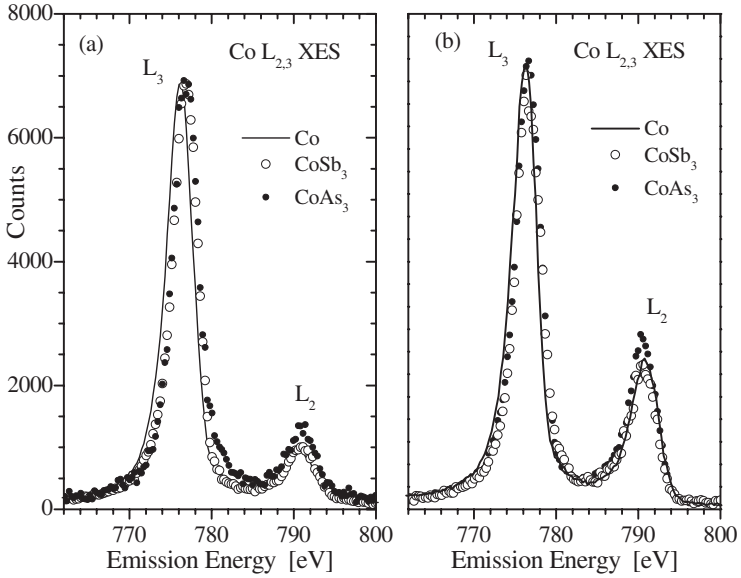

Figure 4. Co $L_{2,3}$ XES of Co, $CoAs_3$ and $CoSb_3$ at (a) non-resonant ($E_{exc} = 841.2$ eV) and (b) resonant ($E_{exc} = 794.5$ eV) excitation.

about 3 eV and the Sb 5p states dominate near the Fermi level. This could be a possible reason for the higher mobility of carriers in $RhSb_3$ and its higher electrical conductivity. At about 10 K this material loses its semiconducting properties and therefore is not considered thermoelectric. The presence of Co 3d states near the Fermi level provides semiconducting properties for temperatures above room temperature. For $CoSb_3$ the first 3d feature resides closer to the Fermi level (∼0.6 eV) compared to that of $CoAs_3$ (∼1.0 eV) and has a higher total density of states (∼50 states eV^{-1}/cell) than $CoAs_3$ (∼40 states eV^{-1}/cell) and $RhSb_3$ (∼10 states eV^{-1}/cell). We note that the energy spread between the highest occupied and lowest unoccupied 3d states is smaller for $CoSb_3$ (∼1.1 eV) than for $CoAs_3$ (∼1.4 eV). These probably are the most favourable conditions for the formation of higher S and σ in $CoSb_3$.

We find the calculated results in good agreement with the measured valence band spectra of $CoAs_3$, $CoSb_3$ and $RhSb_3$ as displayed in figure 5. As 4p and Sb 5p states as well as As 4s and Sb 5s states are labelled by arrows in the calculated spectra. Most noticeably, both are present in the experimental XPS valence spectra with the same energy separation from the main maximum of the Co 3d band as in our calculation. Other As 4p and Sb 5p features with smaller (negative) energies are located in regions with higher contributions of Co 3d states and therefore are found in XPS measurements (figure 5) as weak spectral features arising from Co 3d bands. It is well known that the energy positions of the constituents valence bands are not reproduced by LDA calculations when d–d electron correlation effects are strong, for instance in copper oxides. Therefore the good agreement between XPS and the calculations indicates that electron correlations are not important for the Co compounds and that the electronic structure of these materials is sufficiently well described in the LDA approach.

The efficiency of the material for thermoelectric applications can be estimated by its (dimensionless) figure of merit $Z = \sigma S^2/\kappa$. On the basis of our band structure calculations we have calculated the Seebeck coefficients S using the formula [19] assuming the scattering

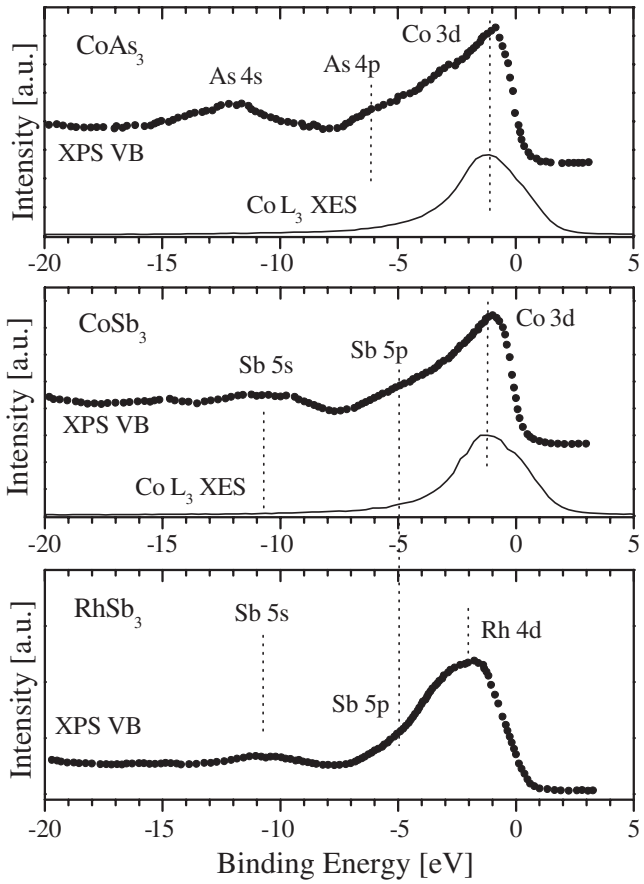

Figure 5. Comparison of XES and XPS VB of $CoAs_3$, $CoSb_3$ and $RhSb_3$ in the binding energy scale.

of electrons by acoustic phonons:

$$S = -\frac{k_B}{e}\left[\frac{2F_1(\eta)}{F_0(\eta)} - \eta\right],$$

where k_B is the Boltzmann factor, e stands for the electron charge, η_n is the reduced Fermi level of the electrons,

$$\eta = (E_F - E_C)/kT,$$

where E_F is the electron Fermi energy and E_C is the lower edge of the conduction band. $F_0(\eta)$ and $F_1(\eta)$ are the Fermi integrals:

$$F_0(\eta) = \int_0^\infty \frac{dx}{1+\exp(x-\eta)} \qquad \text{and} \qquad F_1(\eta) = \int_0^\infty \frac{x\,dx}{1+\exp(x-\eta)},$$

which represent zero and first moments of the electron density of a free gas.

We then use experimental values for σ at room temperature in order to estimate the value of the 'power factor' σS^2, which is proportional to the figure of merit Z and determines the main electron contribution to Z. Table 3 displays that $CoSb_3$ has a higher value for σS^2 than $CoAs_3$ and therefore is likely to be a more promising candidate for thermoelectric applications.

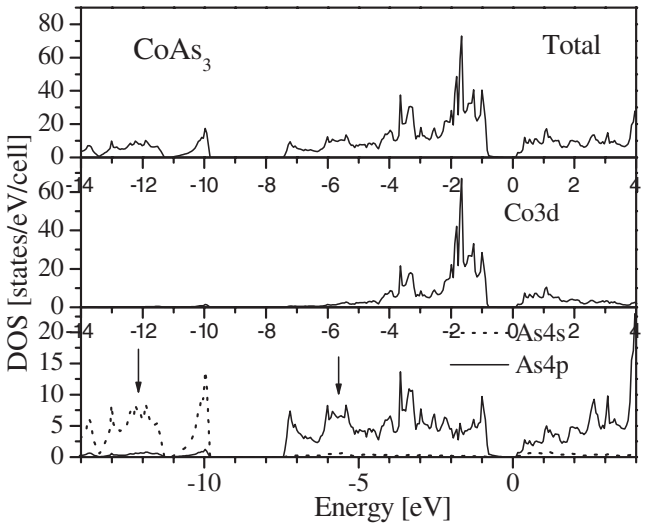

Figure 6. The band structure of $CoAs_3$.

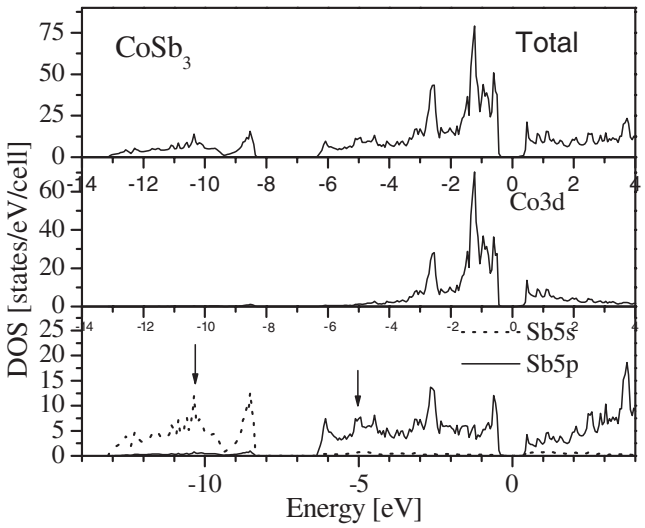

Figure 7. The band structure of $CoSb_3$.

To conclude, we have performed *ab initio* band structure calculations, which we compare with measured valence band spectra of $CoAs_3$, $CoSb_3$ and $RhSb_3$. According to our analysis, the density of states and location of the d peak with respect to the Fermi level and also the energy interval from this peak to the first vacant d peak are very important for the thermoelectric properties of transition metal skutterudites. The conditions most favourable for thermoelectricity are observed in $CoSb_3$ where the 3d peak is located very close to the Fermi level and it has a high density of states leading to the highest thermoelectric figure of merit Z. The differences in electronic structure of $CoSb_3$ and $CoAs_3$ are probably due to different localization of the valence As 4p and Sb 5p states. Comparing our band structure calculations and our measurements provides the correlation between the electronic structure and thermoelectric properties of cobalt antimonide.

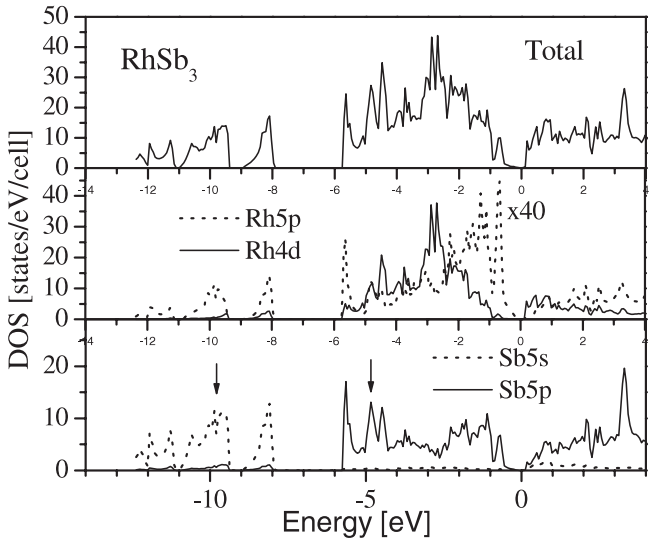

Figure 8. The band structure of $RhSb_3$.

Acknowledgments

Funding by the Research Council of the Presidency of the Russian Federation (Grant NSH-1026.2003.2) and the Natural Sciences and Engineering Research Council of Canada (NSERC) is gratefully acknowledged. The work at the Advanced Light Source at Lawrence Berkeley National Laboratory was supported by US Department of Energy (Contract DE-AC03-76SF00098).

References

[1] Goldsmid H J 1986 *Electronic Refrigeration* (London: Pion)
[2] Tegus O, Brück E, Buschow K H J and de Boer F R 2002 *Nature* **415** 150
[3] Caillat T, Borshchevsky A and Fleurial J-P 1996 *J. Appl. Phys.* **80** 4442
[4] Anno H, Matsubara K, Notohara Y, Sakakibara T and Tashiro H 1999 *J. Appl. Phys.* **86** 3780
[5] Dudkin L D 1958 *Zh. Tekh. Fiz.* **3** 240
Dudkin L D 1958 *Sov. Phys.—Tech. Phys.* **3** 216 (Engl. Transl.)
[6] Singh D J and Pickett W E 1994 *Phys. Rev.* B **50** 11235
[7] Sofo J O and Mahan G D 1998 *Phys. Rev.* B **58** 15620
[8] Caillat T, Borshchevsky A and Fleurial J-P 1996 *J. Appl. Phys.* **80** 4442
[9] Anno H, Matsubara K, Caillat T and Fleurial J-P 2000 *Phys. Rev.* B **62** 10737
[10] Arushabov E, Respaud M, Rakoto H, Broto J M and Caillat T 2000 *Phys. Rev.* B **61** 4672
[11] Nagano J, Ferhat M, Anno H, Matsubara K, Hatta E and Mukasa K 2000 *Appl. Phys. Lett.* **76** 3436
[12] Matsuura M 2004 at press
[13] Pleass C M and Heyding R D 1962 *Can. J. Chem.* **40** 590
[14] Jia J J, Callcott T A, Yurkas J, Ellis A W, Himpsel F J, Samant M G, Stöhr J, Ederer D L, Carlisle J A, Hudson E A, Terminello L J, Shuh D K and Perera R C C 1995 *Rev. Sci. Instrum.* **66** 1394
[15] Methfessel M and Scheffler M 1991 *Physica* B **172** 175
[16] Savrasov S Y 1996 *Phys. Rev.* B **54** 16470
[17] Skinner H W, Bullen T G and Jonston J 1954 *Phil. Mag.* **45** 1070
[18] Grebennikov V I 2002 *Surface Investigation: X-ray, Synchrotron and Neutron Studies* vol 11 p 41
[19] Sandomirsky V, Butenko A, Levin R and Schlesinger Y 2001 *J. Appl. Phys.* **90** 2370